buildings

MDPI

Article

Experimental Investigation on the Rehabilitation of RC Flat Slabs Using CFRP Sheets to Enhance Punching Shear Capacity

Mohammed Qusay Abdul Sahib [1], Reza Aghayari [1,*], Mohammad Javad Moradi [2] and Mehrzad Tahamouli Roudsari [3]

[1] Department of Civil Engineering, Faculty of Engineering, Razi University, Kermanshah 6714414971, Iran; qqmohammed76@gmail.com
[2] Department of Civil and Environmental Engineering, Carleton University, Ottawa, ON K1S 5B6, Canada; mjmoradi@cmail.carleton.ca
[3] Department of Civil Engineering, Kermanshah Branch, Islamic Azad University, Kermanshah 6714473421, Iran
* Correspondence: reza_agh@razi.ac.ir

Abstract: In this paper, the feasibility of strengthening a flat column–slab connection within the carbon fiber reinforced polymer (CFRP) has been investigated through experimental study. The experimental program includes a set of nine reinforced concrete flat slab specimens. Three unaltered specimens served as control slabs, while an additional six samples were strengthened with various CFRP configurations to enhance their shear capacity. The strain distribution, ductility, punching shear resistance, stiffness, and crack formation were studied. The result of experimental studies showed that in the direct method of strengthening in which two layers of unidirectional CFRP sheets were employed in two opposite directions, the ultimate punching shear resistance improved by 64%, 44.7%, and 15.3%, with respect to the location of the column connection, as compared with the control specimens. In the case of using one layer of unidirectional CFRP strips, the punching shear resistance was enhanced by approximately 16% and 39%, considering the configuration of CFRP sheets and the amount of strengthened and adhesive layers used. Following the outcomes of this research, the application of CFRPs in improving the resistance capacity of flat slabs against the punching shear is considerable. The reported outcomes were compared with the latest provisions of ACI to show the efficiency of the presented strengthening. Finally, a parametric study was performed assuming different loading locations to assess the effect of the loading region on the response of RC slabs. Results indicate that approaching the loading location toward the RC slab supports results of an increase in the load-bearing capacity and a reduction in the ductility of the RC slab.

Keywords: flat slab; punching shear; CFRP strengthening; numerical modeling

Citation: Abdul Sahib, M.Q.; Aghayari, R.; Moradi, M.J.; Tahamouli Roudsari, M. Experimental Investigation on the Rehabilitation of RC Flat Slabs Using CFRP Sheets to Enhance Punching Shear Capacity. *Buildings* **2024**, *14*, 153. https://doi.org/10.3390/buildings14010153

Academic Editor: Francisco López-Almansa

Received: 4 December 2023
Revised: 4 January 2024
Accepted: 5 January 2024
Published: 8 January 2024

1. Introduction

The various advantages of the flat slabs, such as user-friendliness, ideal surface finish, and absence of pendant joists, along with reducing the construction time, made this system an appropriate structural system regarding the roof applications [1]. Despite these benefits, the greatest challenge to this design is how to improve the resistance against punching shear. Brittleness and being followed by an unexpected reduction in load-bearing without any previous warning are the main concerns for this type of failure. Therefore, such an unacceptable failure should be prevented [2,3]. Various methods have been suggested for rehabilitating reinforced concrete (RC) flat slabs to enhance their punching shear capacity. These approaches include stirrup shear reinforcement, involving the post-installation of steel bolts in the slab [4–7]; shear studs, employing vertical bars welded at their tops to square anchor heads and at the bottom to a steel strip [8–10]; shear heads, welded to the column and inserted between the layers of the reinforcement [11–13]; shear bolts, similar to

shear stirrups [14–16]; fiber reinforced polymer (FRP) fan, involving FRP rods drilled into the slab's thickness [17–21]; and FRP sheets, attached to the bottom of the slab [22–25].

Failure owing to the punching shear in slab–column connections has a complex nature and becomes more complicated when the unbalanced moment, due to span discontinuity or lateral load, needs to be transferred from the slab to the column, which cannot be circumvented at edge slab–column connections. An imbalanced moment results in an asymmetrical distribution of shear forces, affecting the punching shear strength of connections between edge slabs and columns [26]. Most building codes incorporate a reduction in punching shear capacity, which is typically achieved by decreasing the basic control perimeters, using constant load factors, or assuming a linear or plastic shear distribution along a control perimeter [27]. Although the punching behavior of strengthened reinforced concrete (RC) slabs is studied widely in other research, only limited information is accessible for strengthened exterior or edge slab–column connections. Furthermore, the code provisions are mainly based on experimental results of moment transfer on interior columns. Exterior and edge slab–column connections are assessed in the ACI code using the eccentric shear method. However, the load-bearing capacity of the exterior slab–column connections is notably undervalued using this method [28–32]. Hence, the ACI code adopts an improved strength model, which is derived from experiments conducted on exterior connections. In this model, the unbalanced moment capacity of the exterior connection is determined solely based on the flexural moment capacity of the designated slab width, without taking into account the impact of eccentric shear [33]. Furthermore, the effect of strengthening these types of connections has not been considered.

This paper aims to investigate the behavior of RC flat slab strengthening against punching shear using FRP strips. Furthermore, the current lack of accessible information on the strengthened exterior or edge slab–column connection is addressed. In addition, the FRP configuration is studied experimentally in order to gain optimum performance. The results of the experimental test are compared with the ACI code to determine the accuracy of the proposed equations for the estimation of the RC slab punching shear capacity. In addition, the FE analysis is performed for a detailed investigation of the response of the RC slab under various loading locations. The nonlinear finite element model of RC slabs is generated using ABAQUS software (https://en.wikipedia.org/wiki/Abaqus). The numerical analysis is compared with the results obtained by experimental outcomes. Results show a satisfactory correlation with experiments, and finally, a parametric study is performed to determine the effect of loading location on the response of the RC slab.

2. Experimental Program

2.1. Material Properties

To achieve a 28-day cylinder compressive strength of 35 MPa, a concrete mix was designed with a maximum coarse aggregate size of 10 mm and a water-to-cement ratio of 0.44. The specifics of the concrete mixtures are provided in Table 1, and at the age of 28 days, the concrete exhibited a compressive strength of 45 MPa, a tensile strength of 2.9 MPa, and a modulus of elasticity of 24,400 MPa. Certainly, while the actual compressive strength of concrete in practical construction may be lower, various numerical and theoretical models exist to assess the load-bearing capacity of a concrete slab based on its compressive strength.

Table 1. Concrete mix proportion.

Mixture	Cement (kg/m^3)	Water (kg/m^3)	Fine Aggregate (kg/m^3)	Coarse Aggregate (kg/m^3)
RC	451	196.5	1090.1	613.2

The slabs were reinforced with a total of eleven 14 mm steel rebars in both the x and y directions, with an equal spacing of 90 mm. This configuration involving the diameter of steel rebar was implemented to ensure a heightened flexural response and prioritize punching shear over flexure [34]. This arrangement resulted in a clear concrete cover of

20 mm. The steel rebar had a yielding stress of 400 MPa and an ultimate stress of 600 MPa. An unidirectional CFRP (Sika Wrap®-301 C) was used as the strengthening material. The manufacturer's guaranteed design properties that were used in this study are given in Table 2. In order to paste the CFRP to the bottom surface of the slabs, a two-component epoxy resin was used.

Table 2. Mechanical properties of CFRP.

Material	Thickness (mm)	Cross Section Area (mm^2/m)	Modulus of Elasticity (GPa)	Tensile Strength (MPa)	Rapture Strain
CFRP	0.167	167	225	4300	0.0191

2.2. Test Specimens

Numerous experimental investigations face challenges due to safety and economic constraints, making them impractical. Conversely, conducting preparations and measurements in full-scale development field experiments is expensive and complex. Scaling down experiments, however, enables the identification of crucial effects, enhancement of engineering design, and validation of physics-based models. These scaled-down experiments contribute to predicting structural dynamic responses across all scales [35]. In this study, a total of nine specimens were created to represent isolated interior, edge, and corner slab-column connections. Each specimen was a 1000 × 1000 × 100 mm square slab. This slab size reflects the typical reinforced concrete slabs constructed in the construction industry and has been employed in various studies conducted previously [36,37]. These specimens, denoted as "Sn-x" were designed, fabricated, and tested. The subscript "n" indicated the loading zone location (1, 2, and 3 denoting interior, edge, and corner loading, respectively, as shown in Figure 1), while "x" represented the specimen series, namely A, B, and C. A load, applied at a rate of 1 mm/min, was exerted on a steel loading plate measuring 150 × 110 mm. The specimens were divided into three series: A-Series, serving as control specimens without any strengthening; B-Series, strengthened multi-directionally with CFRP diagonal strips; and C-Series, strengthened either bidirectionally with CFRP sheets (S2-C and S3-C) or orthogonally with CFRP strips (S1-C).

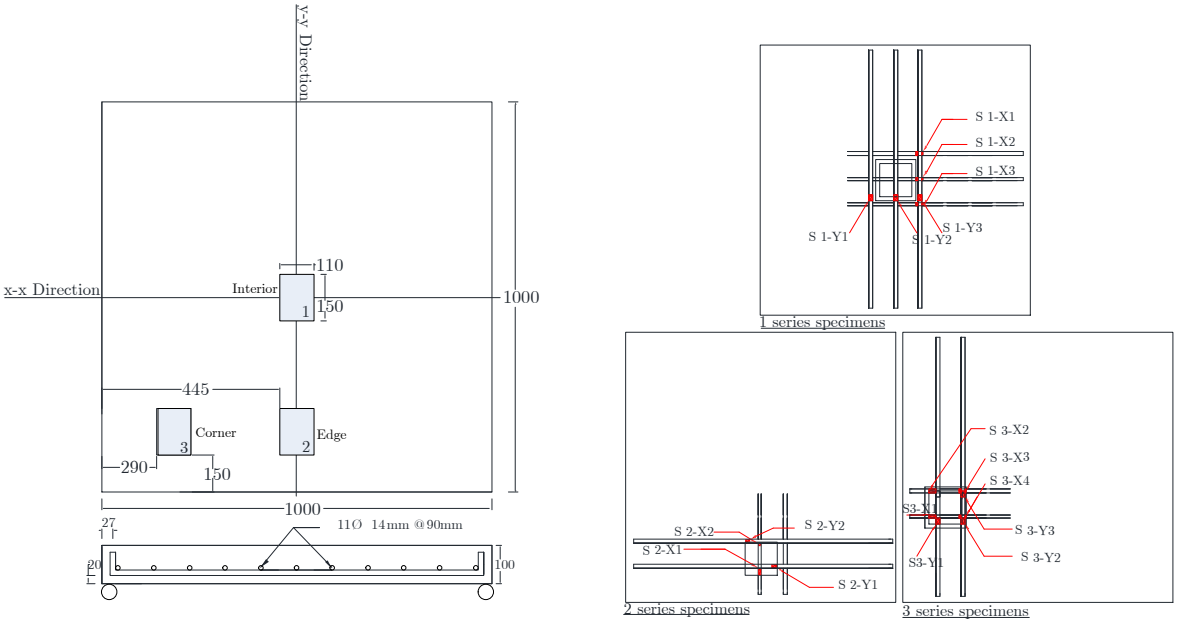

(**a**) (**b**)

Figure 1. (**a**) Specimen geometry and rebar configuration, (**b**) location of loading zone and strain gauges.

In B and C series slabs, CFRP strips with a width of 50 mm and a thickness of 0.167 mm were used for strengthening. The CFRP strips in B-Series extended 90 mm along the slab surface, while in C-Series, they extended 500 mm. The specimen's geometry, rebar layout, loading area position, and strain gauge placement can be observed in Figure 1. Additionally, Figure 2 provides an illustration of the strengthening method and indicates the positions of the strain gauges.

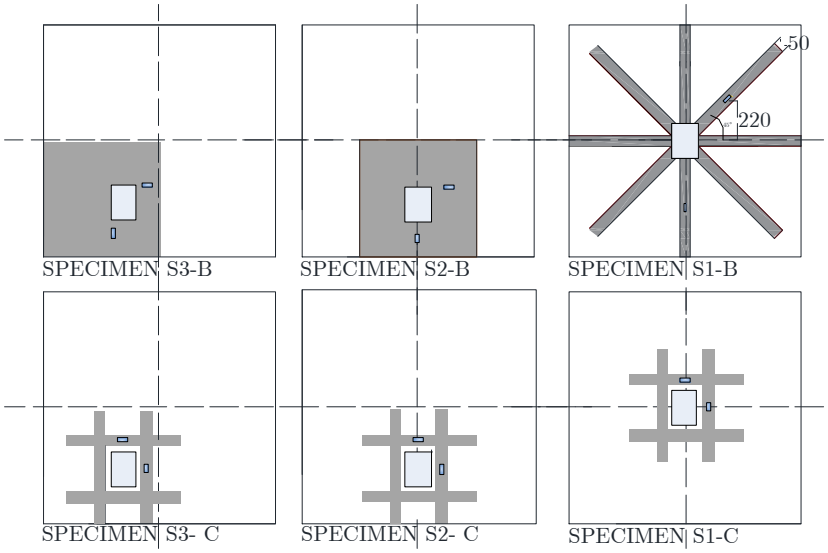

Figure 2. The strengthening technique, along with the location of the strain gauges.

2.3. *Preparation of Test Specimens*

To strengthen the slabs, CFRP strips were affixed to the underside after the slabs had been cured for 28 days in a controlled environment. To ensure a secure bond between the CFRP sheets and the bottom of the slabs, the concrete substrate was first prepared by brushing and leveling its surface. A vacuum cleaner was employed to remove any dust and loose particles from the slab's surface. Both the concrete surface and the CFRP sheets were impregnated with adhesive to prevent the formation of air bubbles. The adhesive layer was created using Sikadur®-330 epoxy matrix, with a mixing ratio of component A to component B at 1:4 by weight. The CFRP sheets were manually applied to the underside of the slabs, ensuring adhesion without compromising the necessary adhesive thickness of 3 mm, as per the guidelines in the Concrete Society Technical Report [38]. To ensure effective contact between CFRP and the concrete surface and eliminate air bubbles in the epoxy, gentle pressure was applied using a roller. Subsequently, the epoxy resin underwent curing to achieve optimal adhesion.

2.4. *Experiment Procedure and Instruments*

The complete reinforced concrete (RC) slabs underwent monotonically controlled loading at a rate of 1 mm/min. The specimens received support at all four edges, as illustrated in Figure 3. To apply the punching load, a hydraulic jack with a capacity of 2500 kN was utilized. This hydraulic jack operated against a reaction frame, which exerted force on a rectangular steel plate measuring 150 × 110 mm.

For ease of testing, the slab specimens were evaluated in an inverted position. This implies that stress in the connection area was induced on the bottom surface of the slab, contrary to the typical arrangement in flat plate construction connections subjected to gravity loads, where stress is induced on the top surface. This approach has been previously employed in various studies [26,39–41]. The deformation response of the RC slab was tracked using a linear variable differential transformer (LVDT) positioned at the center. Strains in the steel reinforcement were measured through strain gauges strategically placed, as depicted in Figure 1b.

Moreover, as depicted in Figure 2, three extra strain gauges were attached to the CFRP sheets to ascertain the mean longitudinal strain in the strengthened specimens. The loading rate was regulated, and a data acquisition system connected to a personal computer was utilized to gather test data, encompassing load, deformation, and strains.

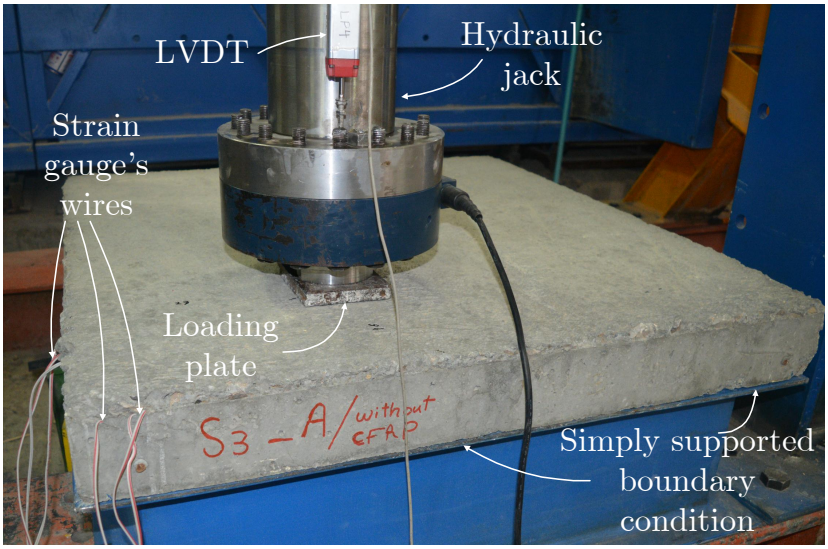

Figure 3. Test setup of experimental specimens.

3. Finite Element Model and Validation

To ensure the accuracy of the numerical results obtained from the finite element software, an experimental slab specimen subjected to static loading is replicated and assessed using the commercial finite element analysis (FEA) software ABAQUS Explicit. The geometry of the RC slab is identical to the experimental slab and is meshed in 3D using *C*3*D*8*R* solid elements. This element is a 3D eight-node linear brick element with reduced integration. The "R" in C3D8R stands for "Reduced Integration", which means that this element uses reduced integration to improve its performance in certain situations [42,43]. The steel rebar is modeled using wire elements, and *T*3*D*2 elements are used for meshing them. This element is a three-node linear triangular element that is used for modeling two-dimensional (2D) structural and plane stress problems. It is often employed in plane stress or plane strain analyses where the out-of-plane deformation is negligible [44]. In the finite element analysis, the steel material exhibits a constitutive behavior characterized by a bi-linear relationship, adhering to an elastic, perfectly plastic model in both tension and compression. The interaction between the steel bar and the surrounding concrete is treated as a constraint within the "embedded region" [45].

A concrete damaged plasticity (CDP) model is adopted to represent the uniaxial compressive and tensile response of the concrete. This model accounts for stiffness degradation due to tensile and compressive failure, as well as concrete damping. One of the distinctive features of the CDP model is its ability to model damage evolution in concrete. The model incorporates a damage variable that evolves with loading, representing the initiation and progression of cracks in the material [46]. The stress–strain relationships are governed by a scalar damaged elasticity equation, as described in Equation (1), where E_c represents the modulus of elasticity of concrete, and σ, ε, ε^{pl}, and d represent (compressive or tensile) stress, strain, plastic strain, and the damage parameter, respectively [47].

$$\begin{cases} \sigma_c = E_c(\varepsilon_c - \varepsilon_c^{pl})(1 - d_c) \\ \sigma_t = E_c(\varepsilon_t - \varepsilon_t^{pl})(1 - d_t) \end{cases} \quad (1)$$

Certain parameters, including the compressive strength and tensile strength of concrete, as well as the tensile strength of steel rebar, were determined through experimental tests. Concrete exhibited a compressive strength of 45 MPa, a tensile strength of 2.9 MPa,

and a modulus of elasticity of 24,400 MPa. The steel rebar had a yielding stress of 400 MPa and an ultimate strength of 600 MPa. However, other parameters essential for modeling the RC slab in ABAQUS were derived from theoretical values based on previous research. The shape factor, denoted as K_c, represents the ratio of the second stress invariant for tension and compression at the same hydrostatic stress and governs the shape of the yield surface. For normal concrete, the default value of K_c is 0.667. Another crucial parameter is the ratio of biaxial to uniaxial compression stress ($\frac{\sigma_{b0}}{\sigma_{c0}}$), which describes the material state during biaxial compression. In the CDP model, the dilation angle (ψ) and the flow potential eccentricity (ϵ) play a significant role in defining the potential plastic flow of concrete under a three-dimensional stress state. The dilation angle represents the change in volumetric strain during plastic deformation. The flow potential eccentricity signifies the rate at which the flow function approaches the asymptote. The viscosity parameter is an additional factor employed to define concrete in ABAQUS, aimed at enhancing the convergence rate during simulations [26,48]. For this parameter, it is recommended to use a small value to improve the convergence rate [49] or use 0 [50].

As reported by Daneshvar et al. [51], they specified the dilation angle (ψ) as 56, plastic potential eccentricity (ϵ) as 0.1, the ratio of biaxial stress to uniaxial stress ($\frac{f_{b0}}{f_{c0}}$) as 1.16, the ratio of the second stress invariant on the tensile meridian, which is known as shape parameter (K_c), as 0.66, and viscosity parameter (μ) as 0. The essential input parameters for modeling concrete in ABAQUS are summarized in Table 3. Given that the specimen supports were constructed using high-strength steel and exhibited no noticeable deformation during testing, they were modeled as rigid body elements in the numerical models [52]. The boundary conditions for the model were set to simulate simple support at all four sides. Furthermore, the loading plate was represented using rigid elements and was not included in the slab model itself. The simulation of the loading plate and concrete contact problem involves employing surface-to-surface interaction with the hard contact property, utilizing a penalty contact formulation. Using the hard contact, the stress and the resulting displacement are fully transmitted to the slab [53].

Table 3. The essential input parameters for modeling concrete in ABAQUS.

Dilation Angle	Eccentricity	$\frac{\sigma_{b0}}{\sigma_{c0}}$	K_c	Viscosity Parameter	Poisson Ratio
56	0.1	1.16	0.66	0	0.2

Given that the predominant failure modes observed in the experimental specimens were concrete crushing and punching shear, the CFRP sheets were represented in the model using shell elements, specifically the *S4R* element. This element is a 4-node element with six degrees of freedom at each node—three displacements and three rotations—utilizing a transverse shear strain field in its formulation [54]. To connect the CFRP sheets to the RC slabs in ABAQUS, a "Tie" constraint was employed. In ABAQUS, the "Tie" constraint is a type of constraint that is used to simulate the bonding or connection between two surfaces or sets of nodes. It is often employed in contact analysis to model interactions between different parts of a structure.

Validation

To ensure the accuracy of the numerical simulation, a comparison between numerical and experimental results was conducted. Figure 4 illustrates the load–deflection curves, revealing a satisfactory agreement between the experimental specimens and numerical models. Discrepancies between the numerical and experimental findings can be attributed to factors such as the finite element model's characteristics, the degree of concrete heterogeneity, assumptions made in the analysis, and the chosen boundary conditions. The reasonable agreement enhances confidence in the reliability of the numerical models, potentially allowing for an expanded scope of models and parameters in a parametric study. Table 4 provides a summary of errors in predicting the ultimate load-bearing capacity of

RC slabs using numerical models. The average error across all cases is 1%, with the highest error observed in S2-A numerical models, reaching nearly 10% in predicting the ultimate load-bearing capacity.

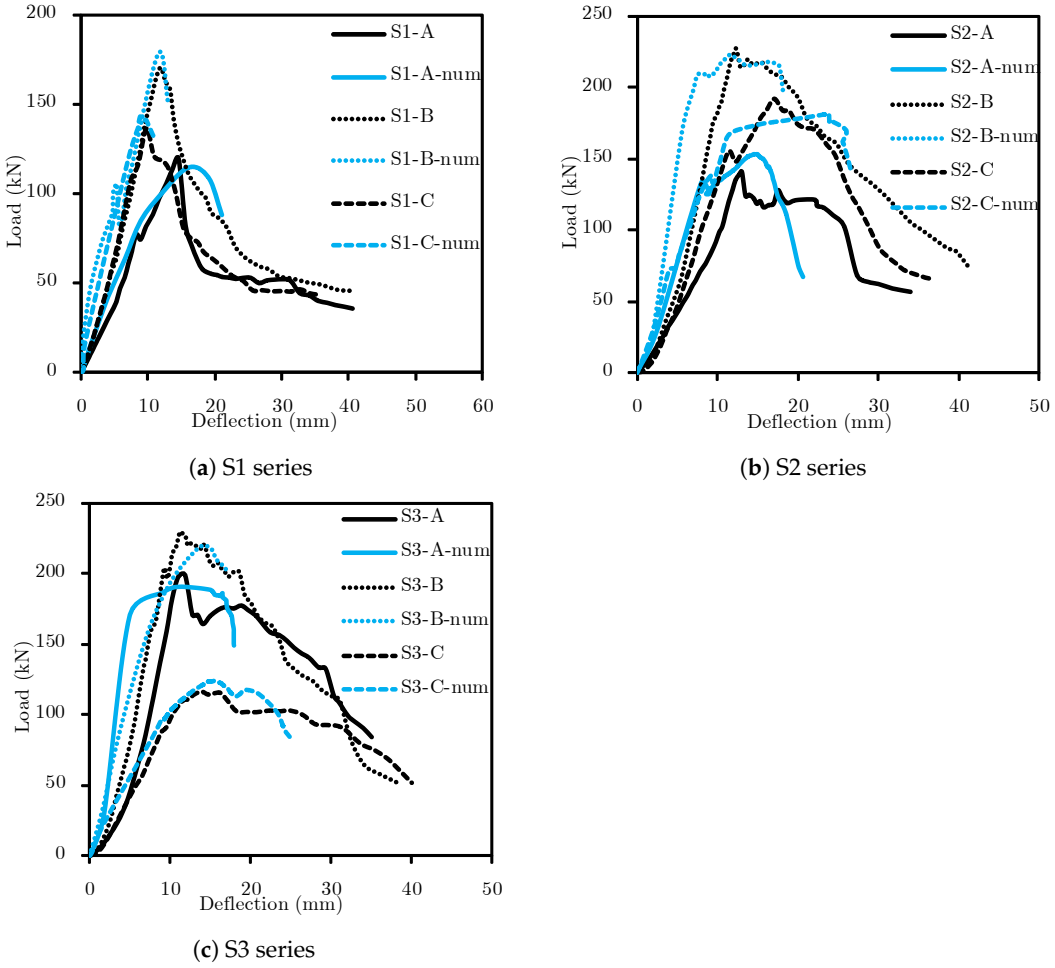

(**a**) S1 series (**b**) S2 series

(**c**) S3 series

Figure 4. Load–deflection of the various slabs, along with their numerical results.

Table 4. The essential input parameters for modeling concrete in ABAQUS.

Specimen	V_u Experimental (kN)	V_u Numerical (kN)	$V_{u(exp.)}/V_{u(num.)}$
S1-A	117.232	114.5	1.02
S1-B	169.71	178.2	0.95
S1-C	135.94	143	0.95
S2-A	138.28	153.1	0.90
S2-B	226.07	223	1.01
S2-C	191.249	181.5	1.05
S3-A	198.215	190.5	1.04
S3-B	228.612	218.6	1.04
S3-C	116.2	123.9	0.93

4. Results and Discussion

4.1. Failure Characteristics

All of the tested specimens failed in a brittle punching shear mode but at various load levels depending on the quantity of CFRP. However, the ultimate load and the first crack had diverse responses. The first noticeable crack was detected on samples S1-A, S2-A, and S3-A, at a load of 39.3, 32.6, and 25.2 kN, respectively. This crack appeared near the loading plate, and with an extension in the applied load, the cracks propagated, and the

loading plate penetrated into the slab. The tension cracks in the bottom of the slabs were entered within the thickness of the slab towards the compression surface with an increase in the concentric load. The slab was divided into two separate parts due to the propagation of the cracks on the vertical surface of the slab-free edge (Figure 5a). Due to a lack of experimental equipment, the authors were unable to cut the slab and examine the section view. In situations where conducting experimental tests is challenging or measurements are difficult to obtain, numerical modeling can be a valuable and helpful alternative [55,56]. The numerical models are able to capture the cracking pattern, as depicted in Figure 5b. The progression of cracks persisted, extending through the thickness of the slab until concrete crushing occurred at the top surface of samples S1-A, S2-A, and S3-A. This took place in the proximity of the column at loads of 119.5 kN, 140.8 kN, and 198.9 kN, respectively. Notably, a reduction in load corresponding to the initiation of the first crack was observed, accompanied by an increase in the ultimate load. This phenomenon was attributed to the column being positioned closer to the edge of the slab.

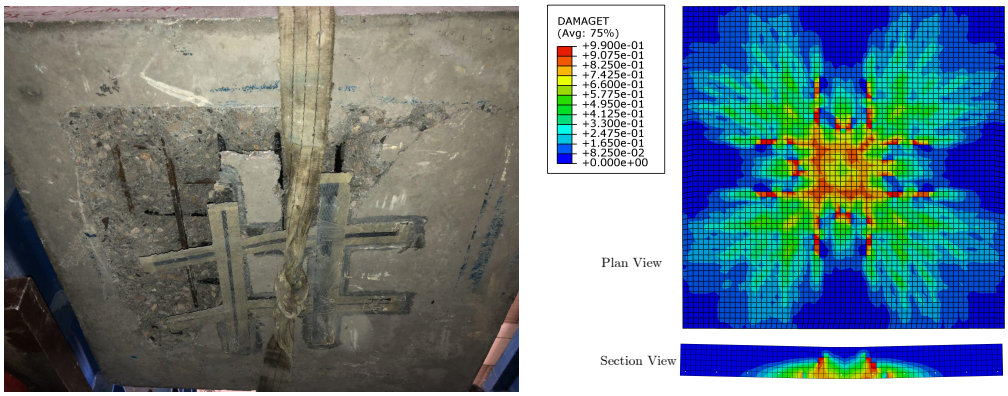

(**a**) (**b**)

Figure 5. Cracking pattern in (**a**) numerical model, and (**b**) experimental specimen.

The deformation, cracking loads, and ultimate loads are listed in Table 5. The steel-yielding load (P_y) represents the load level in which the first rebar yields, and its corresponding deflection, which is denoted by Δ_y, is summarized in Table 5. Moreover, the ultimate load and its corresponding deformation signified by P_u and Δ_u, respectively, are listed in Table 5. The strengthened specimens exhibited a similar mode of failure as the unstrengthened specimens. Failure started outside the strengthened zone, followed by the penetration toward the loading zone but with a lag in the presence of apparent cracks. The first noticeable cracks at the slab edge were noted at the cracking loads that are listed in Table 5.

In comparison to the control specimens, the strengthened slabs exhibited an increase in ultimate load when the column was displaced towards the edges of the slab. It is obvious that the CFRP sheets led to an improvement in the load-bearing capacity until the bond between the bottom surface of the slab and CFRP sheets failed. This can be attributed to the additional tensile strength and confinement provided by the CFRP reinforcement. There was neither detected a failure in CFRP sheets nor the development of the epoxy bond-lines except in specimen S3-C. The CFRP debonding can be attributed to the concrete crushing, which leads to peeling off the CFRP sheet (Figure 6). The failure strain was 0.51%, which is almost 26% of the CFRP rupture strain. Localized cracks developed at the following step of loading owing to the expansion of the diagonal shear and the flexural cracks, which caused the CFRP sheets separation. These cracks were positioned adjacent to the edges of the CFRP sheet's length.

Table 5. Summary of test results on RC slabs.

Slab	P_{cr}	P_y	P_u	Deflection		Ductility
	Exp.	Exp.	Exp.	Δ_y	Δ_u	μ
S1-A	18.8	79.9	119.5	4.48	45.41	10.1
S2-A	44.3	101.9	140.8	5.25	34	6.5
S3-A	84.8	136.1	198.9	6.93	35.07	5.0
S1-B	75.3	141.4	170.3	5.89	40.2	6.8
S2-B	163.3	196.5	226.8	9.07	41.24	4.5
S3-B	162.7	190.6	229.4	8	38.29	4.7
S1-C	58.2	90.5	136.4	4.56	35.04	7.7
S2-C	65.4	128.7	191.9	6.12	36.96	6.0
S3-C	56.7	–	116.2	6.55	40.05	6.1

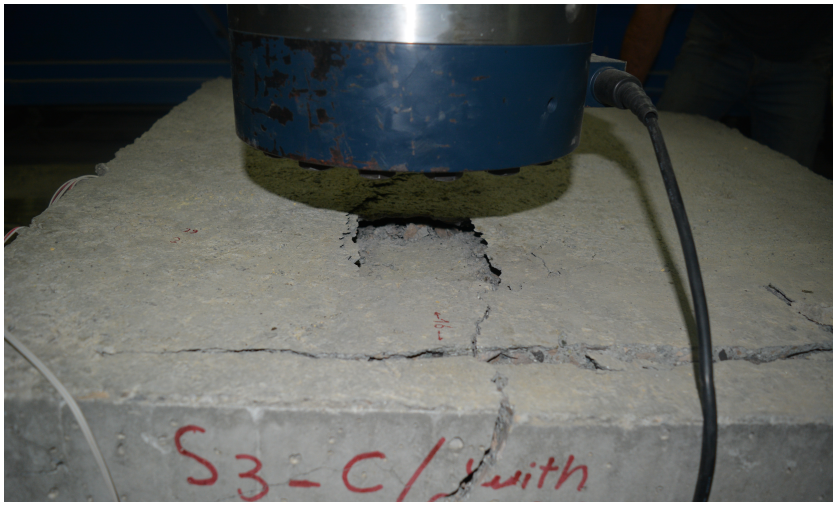

Figure 6. Crushing in the concrete of specimen S3-C.

The ductility for each specimen can be determined as the division of ultimate and the yield vertical displacement, i.e., $\mu = \frac{\Delta_u}{\Delta_y}$. As can be seen in Table 5, an increase in column eccentricity in control specimens results in a reduction in ductility. Ductility was obtained as 10.1, 6.5, and 5.0 for specimens S1-A, S2-A, and S3-A, respectively. The reason for a decrease in ductility can be attributed to higher yield deflection and lower ultimate deflection due to the shifting of the loading region to the supports. This conclusion follows the findings of other researchers as the ductility reduced because of CFRP application for strengthening RC slabs [1,23,26,57,58]. However, the ductility is less under the influence of the column eccentricity in strengthened slabs. Since the CFRP sheets limit the tendency of the slab to undergo relatively wide cracks after yielding of rebar and also increase the out-of-plane stiffness of the interior slab-column connection, eventually reduce the ultimate deflection, Δ_u and increase the yielding deflection, Δ_y, compared to the control slab. Thus, the strengthening specimens behave fairly similarly, and the reduction in ductility decreases.

4.2. Load–Deflection Characteristics

In this section, the effectiveness of punching rehabilitation for various strengthening patterns is assessed by investigating the results acquired in the experimental test. The performance of the strengthening technique was evaluated in terms of load-bearing capacity. The load–displacement curves at the center of the various slab series are shown in Figure 7. The load–deflection behavior of specimens was nearly linear before any cracking happened in the section resulting in high stiffness. After the initial crack formation, the slab's behavior was primarily influenced by the reinforcement and the strengthening method. The appearance of the first circular crack around the column led to a sudden reduction in the stiffness

of the control slab. This may cause subsequent deep and wide flexural cracks throughout the negative moment zone. This can lead to a further stiffness reduction. After that, an almost linear relationship is expected between the deflection and load, up to the ultimate load, while the existing cracks widen and propagate towards the area of compression load. In general, from Figure 4, it can be seen that at a specific load level, the presence of the CFRP sheets results in a reduction in the slab deflection. This reduction is due to the contribution of the CFRP strips in improving flexural stiffness and rotational resistance of the slabs by confining the diagonal shear crack and limiting crack opening.

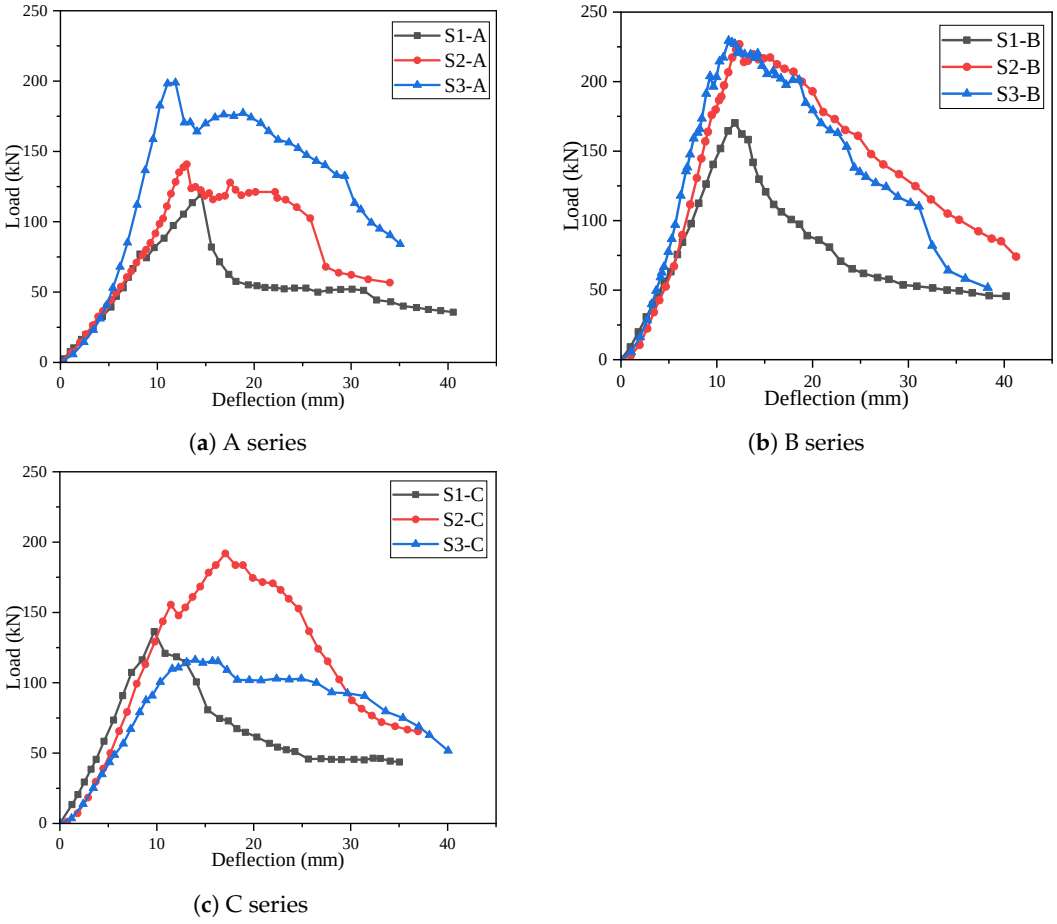

Figure 7. Load–deflection curves of different specimens with various types of strengthening.

The strengthened specimens S1-B and S1-C showed a less ductile failure behavior. The central displacement corresponds to the ultimate load for S1-B and S1-C was 11.89 and 9.74 mm, respectively, when compared to the deflection of the control specimen, i.e., 14.54 mm, which indicates an 18.2 and 33% reduction. This can be attributed to the confinement effect of CFRP sheets in restricting the propagation and opening of cracks, leading to a small decrease in the slab central displacement compared to the control slab at the identical load level. Moreover, the slope of the load–deflection curves was higher compared to the control specimen (S1-A). Since no FRP debonding in these specimens was observed during the tests, no reduction in the stiffness of strengthened specimens can be seen in load–deflection curves.

The failure loads of the S1-B and S1-C specimens were higher than the control slab. The presence of CFRP in S1-B and S1-C specimens led to a 42.5 and 14.2% increase in peak load compared to the S1-A slab, respectively. It is observed that the strengthening technique has a notable effect on the punching shear capacity of interior slab–column connections. S1-B and S1-C specimens failed at 170.3 and 136.4 kN, respectively. The quantity of CFRP sheets employed in specimen S1-B exceeded that used in S1-C. The

same trend for edge slab–column connections (S2 series) was observed. The ultimate load of S2-B and S2-C was 61 and 36.3% higher than their control slab, respectively. The increase in the ultimate load of strengthened specimens of the S2 series was higher than the S1 series, which indicates the greater efficiency of strengthening in edge slab–column connections compared to interior connections. In addition, in both series, the effect of type-B strengthening was more significant. This can be attributed to the higher amount of epoxy resin that delays the debonding tendency of CFRP sheets. Debonding of the CFRP sheets in S3-C specimens results in a 41.5% reduction in load-bearing capacity compared to the control specimen. In these specimens, strengthening using CFRP sheets and confining all around the loading region may result in an increase in load-bearing capacity as well as enhancement in the initial stiffness of the slab compared with the S3-A slab. These improvements in load-bearing capacity and initial stiffness are 15.3% and 86% compared to the control specimen.

4.3. Strain Measurements

Several strain gauges were used to measure the strain of CFRP sheets and steel rebar, as shown in Figures 1b and 2. The steel strains in all specimens are plotted in Figure 8a–i. It can be seen that S1-A is the only specimen whose steel rebar did not yield prior to failure. The steel strain in other specimens is generally greater than the typical value of the 2000 microstrain used as the yield strain of reinforcing steel. Similar outcomes were noted in [59,60]. It is obvious that the existence of CFRP sheets in 2 and 3 series compared to 1 series results in a reduction in steel strains at a given load due to the contribution of these materials in improving the strength and out-of-plane stiffness of the slab as well as relieving some tensile stresses in the steel rebars, as compared to those for the control specimens. Beyond the yielding point, a subsequent change in the slope of the curve occurred, indicating the initiation of a new stage of deformation characterized by plastic deformation. During this phase, the strain increased rapidly with a slight concurrent increase in the load. Due to improper installation and the increasing formation of cracks along with their widening, the strain gauges became detached during the tests. This is one of the reasons for changing the direction of strain measurement. The other reason, which is obvious in Figure 8b,e–i, is a structural failure, which can alter the direction of strain as the material undergoes changes in its internal stress distribution.

The CFRP sheet strain is shown in Figure 9. It can be understood that all the strain measurements have a nearly horizontal and immediate change at a certain load level, which implies that the shear crack has crossed the location of the strain gauges. At the early stages of loading, 3-series specimens recorded fewer strains than other slabs because the development of cracks in the loading region was postponed due to the vicinity of the loading plate to the supports.

4.4. Stiffness and Energy Absorption of the Slabs

The stiffness and energy absorption of the RC slabs can be determined using load–deflection curves. The initial slope of the equivalent bi-linear curve, which is defined based on an equal energy criterion, is considered as stiffness [61,62]. The energy absorption capacity can be determined by calculating the area under the load–displacement curve [63]. The test results of stiffness and energy absorption are listed in Table 6. Experimental results of stiffness indicate that variation in loading region can significantly affect the stiffness of the slab. In addition, the strengthening results in an increase in out-of-plane stiffness of the RC slabs with an average of 45%. The RC slabs with a central loading region are more susceptible to stiffness enhancement due to strengthening using CFRP sheets. This may be because of the lower out-of-plane stiffness of the unstrengthened RC slab when it is loaded centrally. The same trend can be observed for absorbed energy. Strengthening the RC slabs regardless of loading region causes an average increase of 28.6% in absorbed energy compared to control specimens. However, strengthening using the B series is more effective than the C series in both stiffness and absorbed energy improvement. The percentage of

increase in B series and C series are 61.6% and 28.2% for stiffness and 49.1% and 8.1% for energy absorption, respectively. The main reason for this trend can be explained by the higher amount of CFRP implementation, which reduces the risk of CFRP debonding. Moreover, in the B series, CFRP's mechanical properties contribute to a more uniform distribution of stresses within the structure. This uniformity helps prevent localized stress concentrations that could lead to debonding.

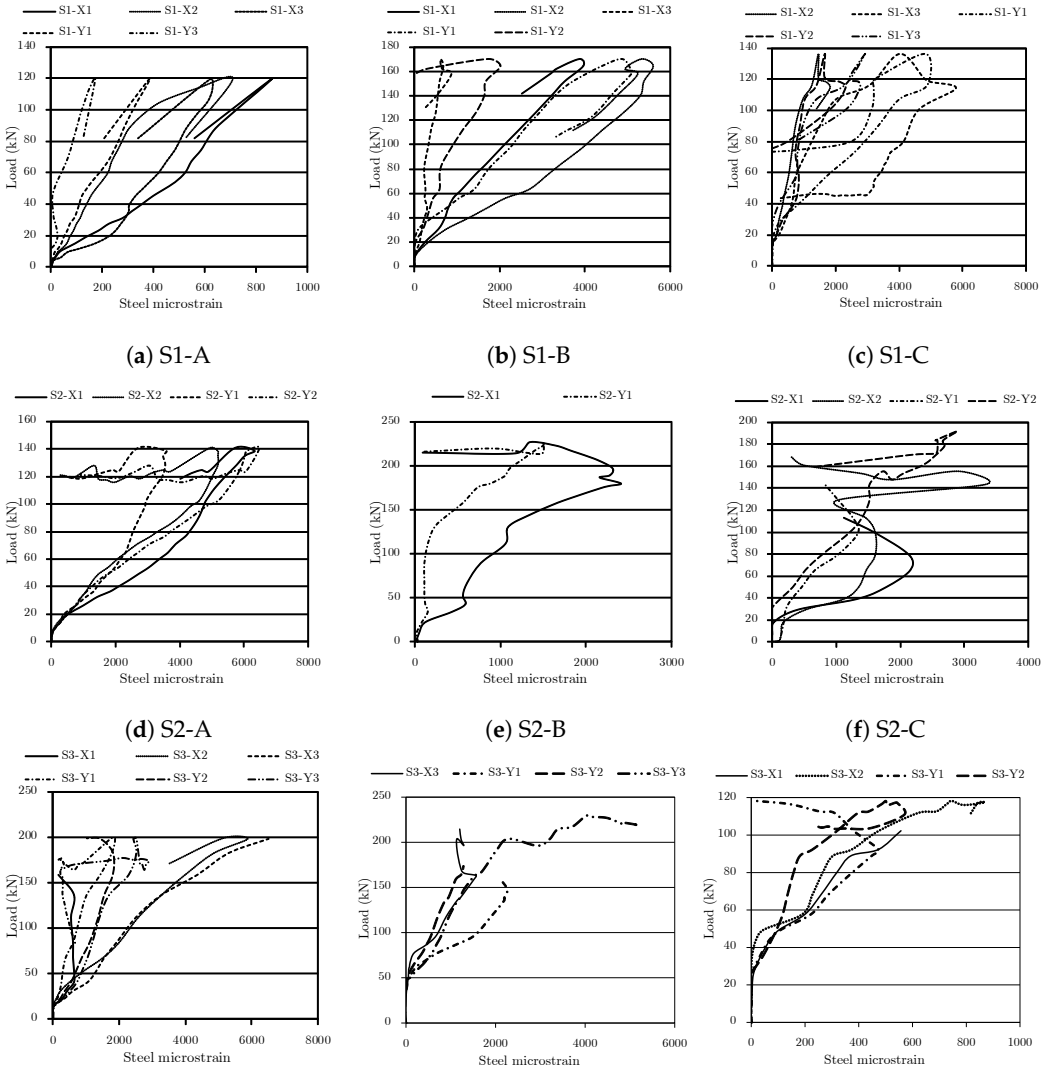

Figure 8. Steel strain distributions in various directions.

Table 6. Experimental results of stiffness and absorbed energy.

Specimen	Stiffness	Absorbed Energy
S1-A	7.54	2226.6
S2-A	11.41	2852.397
S3-A	9.18	4374.004
S1-B	14.02	3106.28
S2-B	12.82	5506.2
S3-B	17.13	5022.38
S1-C	12.8	2323.193
S2-C	12.52	4145.47
S3-C	9.66	3274.237

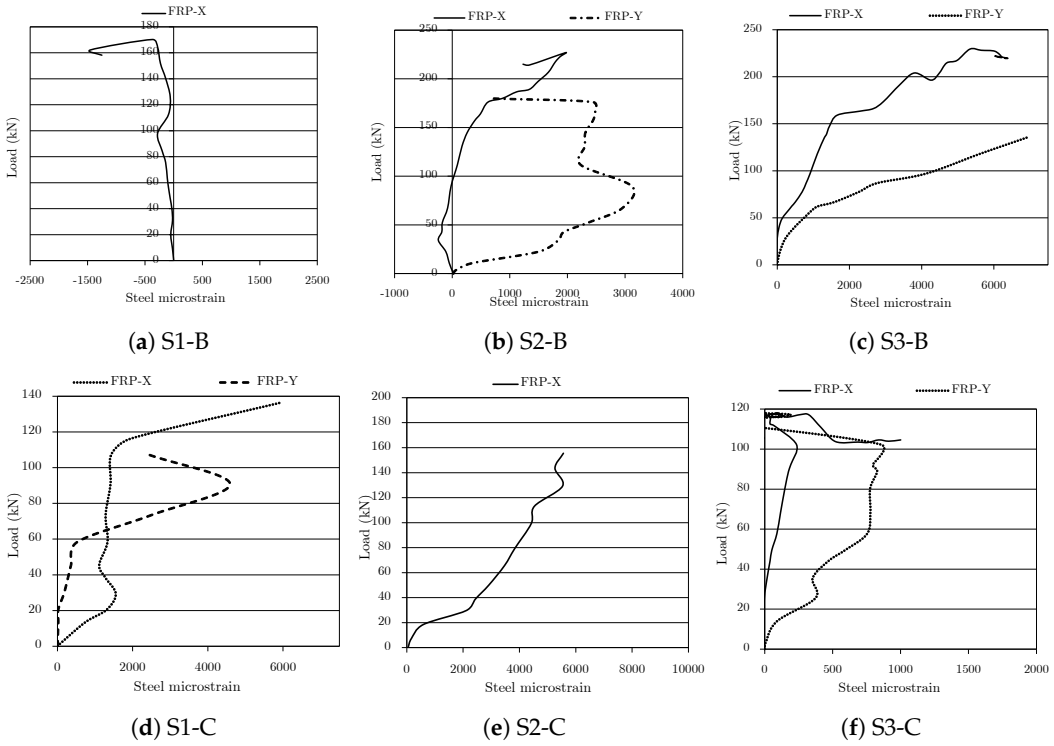

(**a**) S1-B (**b**) S2-B (**c**) S3-B

(**d**) S1-C (**e**) S2-C (**f**) S3-C

Figure 9. FRP sheet strain distributions in various directions.

5. Comparison with Current ACI Code Requirements

Because the ACI 318 code offers design methods for predicting the punching shear capacity of RC flat slabs, the results of the punching shear tests were compared with the values estimated using the punching shear principles outlined in ACI 318 [64]. In the ACI code, punching shear strength can be regarded as the product of the shear strength and the area at the critical section, which is at a specified distance from the column face. The shear strength of the critical section can be represented as Equation (2).

$$v_c = 0.062\left(\beta_p\sqrt{f_c'} + 0.3f_{pc} + \frac{V_p}{b_0 d}\right) \quad (2)$$

In this equation, b_0 stands for the perimeter length of the critical section at a distance equal to half of the slab section from the column face, d is slab thickness, V_p indicates the vertical component of all the effective prestress forces crossing the critical section, and β_p is the ratio of the long side over the short side of the column and needs to be the smaller of 3.5 or $10\left(\frac{\alpha_s d}{b_0} + 0.15\right)$. For an interior, edge, and corner column, α is 4, 3, and 2, respectively. Equation (2) can be implemented for concrete with a compressive strength of less than 35 MPa; otherwise, Equation (3) must be used.

$$v_c = min\begin{Bmatrix} 0.248\sqrt{f_c'} \\ 0.128\sqrt{f_c'}\left(1 + \frac{2}{\beta_c}\right) \\ 0.623\sqrt{f_c'}\left(0.2 + \frac{\alpha_s d}{b_0}\right) \end{Bmatrix} \quad (3)$$

The comparison of experimental test results and design values calculated using the ACI code is listed in Table 7. In this table, the ACI code presents a conservative estimation for RC slabs and is more dominant in the B series, which strengthened the RC slabs with CFRP sheets. In addition, the ACI code methods are able to estimate the punching shear of the unstrengthened RC slab with reasonable accuracy. However, the accuracy of these methods declines with distancing the column from the centerline. In other words, ACI equations cannot precisely estimate the punching shear capacity of an RC slab with an edge

column. The amount of error in predicting the punching shear of unstrengthened edge and corner slab–column connections are 42% and 14%, respectively. The accuracy of the ACI code prediction increased with utilizing CFRP sheets.

Table 7. Comparison of test results with code estimations.

Specimen	$V_{u,experimental}$ (kN)	$V_{u,predicted}$ (kN)	$V_{u,experimental}/V_{u,predicted}$	Increasing with CFRP Sheets (kN)
S1-A	117.23	119	0.985	–
S1-B	169.71	119	1.426	49.71
S1-C	135.94	119	1.142	19.94
S2-A	138.28	119	1.162	–
S2-B	226.07	119	1.899	106.07
S2-C	191.25	119	1.607	71.249
S3-A	198.21	119	1.665	–
S3-B	228.61	119	1.921	108.612

6. Parametric Study on the Location of Loading

By conducting experimental studies and establishing benchmarks for validating finite element models, a pathway has been cleared for subsequent investigations into the punching behavior of strengthened RC slabs. In order to evaluate the influence of loading location on the response of RC slabs, a series of numerical specimens were generated, leading to the development of 35 distinct finite element models. These models were analyzed, and the combined variations in loading location on peak load and ductility were determined for each slab. It's important to highlight that these models exclusively pertain to the present investigation and should not be extrapolated to other comparable components. Figure 10 shows the numerical specimens in a parametric study, where the variation in the location of the loading region is evaluated. The location of the loading region was treated as a variable in both the x and y directions. The variable's range, measured from the center point of the loading plate, spans from 50 to 950 mm, with increments of 50 mm.

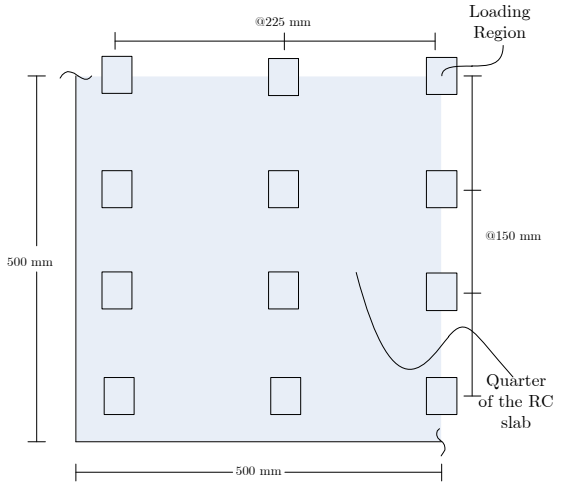

Figure 10. Illustration of numerical specimens for parametric study to investigate the effect of loading region.

Figure 11a indicates that moving away from supports causes a reduction in peak load. Loading closer to the supports creates a leverage effect, allowing the slab to distribute the applied load more efficiently. Moreover, when the load is applied near the midspan of the slab, it generates a higher bending moment at that location. This increased bending moment requires the slab to undergo greater flexural deformation, potentially leading to an earlier onset of failure. In addition, when a load is applied in the middle, the shear forces

are not effectively distributed, leading to higher localized shear stresses and, consequently, punching shear. This type of failure can lead to a reduced load-bearing capacity, especially if the slab is not adequately reinforced around the loading region. Therefore, the expected load-bearing capacity of the RC slab is reduced.

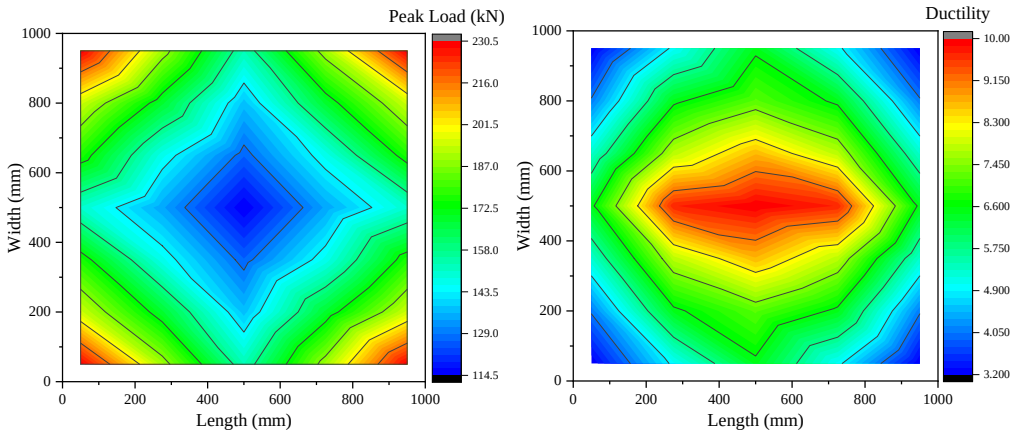

(**a**) Peak Load (**b**) Ductility

Figure 11. Variation in peak load and ductility for different loading locations.

As can be seen in Figure 11b the ductility increases toward the center of the slab, which has the least out-of-plane stiffness. The maximum ductility is about 10 and decreases to less than 3.5 when approaching the loading location toward the RC slab supports. This means that although the peak load and load-bearing capacity of the slab increase with approaching the loading location toward the RC slab supports, the ductility of the slab reduces, and a brittle failure of RC slabs can be expected. Brittle failure in an RC slab refers to a sudden and catastrophic failure with little or no warning before collapse. Unlike ductile failure, where structures show significant deformation and warning signs before failure, brittle failure occurs with minimal deformation, and the structure may fail abruptly. This type of failure results in a rapid loss of load-carrying capacity. This type of failure is typically characterized by the development of multiple, closely spaced cracks that lead to the structural elements' inability to support loads, ultimately resulting in collapse.

7. Conclusions

The implementation of CFRP strengthening at the flat slabs in the first place is to improve punching shear capacity. It is possible to observe a less ductile behavior in strengthening the flat slab, considering the applied configuration for CFRP sheets' strengthening, even after achieving an enhancement in the total load. Following the research outcomes, the prime findings are summarized as follows:

1. The arrangement and quantity of CFRP sheets significantly influenced the performance improvement of flat slabs, leading to an enhancement in punching shear capacity. The results varied among different specimens. Notably, by applying CFRP in a rectangular shape beneath the slab, the load-bearing capacity experienced a remarkable increase, reaching 18.2% and 97% compared to the application of CFRP sheets alone for edge and corner slab–column connections.
2. Strengthening flat slabs by the direct method of surface-mounted CFRP delays the occurrence of the flexural type of cracks in the slab. Such a delay enhances the performance of slabs by improving their ultimate load-bearing capacity. Once two layers from unidirectional CFRP sheets were used in the opposite direction, an increase of ultimate punching shear capacity by 64%, 44.7%, and 15.3% was observed, while in the case of utilizing one layer from unidirectional CFRP strips, strengthening improved the slab's capacity against the punching shear by almost up to 16% and 39%.

3. Within the column region, the steel rebars' total strain is enhanced using externally-bonded sheets of CFRP.
4. The variation in the loading region can significantly affect the stiffness of the slab. In addition, strengthening results in an increase in the stiffness of slabs with an average of 45%. The RC slabs with a central loading region are more susceptible to stiffness enhancement due to strengthening using CFRP sheets. In terms of effectiveness, the percentage increase in stiffness for the B series is 61.6%, while for the C series, it is 28.2%. This suggests that strengthening with the B series is more effective in enhancing stiffness compared to the C series.
5. The utilization of externally applied CFRP sheets in strengthening demonstrates a distinct effect on the strength of flat slabs, particularly in their ability to carry energy within the plastic deformation phase. Strengthening RC slabs, regardless of the loading region, results in an average increase of 28.6% in absorbed energy compared to control specimens. The percentage increase in energy absorption is 49.1% for the B series and 8.1% for the C series.
6. The ACI code provides a conservative estimate for the load-bearing capacity of RC slabs, with decreasing precision as the column is displaced from the slab's centerline. The prediction error for punching shear in unstrengthened edge and corner slab–column connections is 42% and 14%, respectively. Notably, the accuracy of ACI code predictions improves when CFRP sheets are utilized in the strengthening process.
7. The parametric study indicates that approaching the loading location toward the RC slab supports results in an increase in the load-bearing capacity and a reduction in the ductility of the RC slab.

Author Contributions: Conceptualization, M.Q.A.S., R.A. and M.J.M.; methodology, M.Q.A.S., R.A. and M.T.R.; software, M.J.M.; validation, M.J.M.; formal analysis, M.Q.A.S. and M.J.M.; investigation, M.Q.A.S.; resources, R.A. and M.J.M.; data curation, M.Q.A.S.; writing—original draft preparation, R.A., M.J.M. and M.T.R.; writing—review and editing, R.A., M.J.M. and M.T.R.; visualization, M.J.M.; supervision, R.A. and M.T.R.; project administration, R.A. and M.T.R.; funding acquisition, R.A. and M.T.R. All authors have read and agreed to the published version of the manuscript.

Funding: This research received no external funding.

Data Availability Statement: The data presented in this study are available on request from the corresponding author.

Conflicts of Interest: The authors declare no conflict of interest.

References

1. Farhangi, V.; Karakouzian, M. Effect of fiber reinforced polymer tubes filled with recycled materials and concrete on structural capacity of pile foundations. *Appl. Sci.* **2020**, *10*, 1554. [CrossRef]
2. Menétrey, P. Synthesis of punching failure in reinforced concrete. *Cem. Concr. Compos.* **2002**, *24*, 497–507. [CrossRef]
3. Amiri, S.; Talaeitaba, S.B. Punching shear strengthening of flat slabs with EBROG and EBRIG–FRP strips. In *Structures;* Elsevier: Amsterdam, The Netherlands, 2020; Volume 26, pp. 139–155.
4. Broms, C.E. Shear reinforcement for deflection ductility of flat plates. *ACI Struct. J.* **1990**, *87*, 696–705.
5. Elstner, R.C.; Hognestad, E. Shearing strength of reinforced concrete slabs. *J. Proc.* **1956**, *53*, 29–58.
6. Graf, O. Strength tests of thick reinforced concrete slabs supported on all sides under concentrated loads. *Dtsch. Ausschüss Eisenbeton* **1938**, *88*, 22.
7. Oliveira, D.R.; Melo, G.S.; Regan, P.E. Punching strengths of flat plates with vertical or inclined stirrups. *Struct. J.* **2000**, *97*, 485–491.
8. Dilger, W.H.; Ghali, A. Shear reinforcement for concrete slabs. *J. Struct. Div.* **1981**, *107*, 2403–2420. [CrossRef]
9. Elgabry, A.A.; Ghali, A. Tests on concrete slab-column connections with stud-shear reinforcement subjected to shear-moment transfer. *Struct. J.* **1987**, *84*, 433–442.
10. Mokhtar, A.S.; Ghali, A.; Dilger, W. Stud shear reinforcement for flat concrete plates. *J. Proc.* **1985**, *82*, 676–683.
11. Anderson, J. Punching of concrete slabs with shear reinforcement. Royal Institute of Technology. *Bulletin* **1963**, *212*.
12. Corley, W.G.; Hawkins, N.M. Shearhead reinforcement for slabs. *J. Proc.* **1968**, *65*, 811–824.
13. Moe, J. *Shearing Strength of Reinforced Concrete Slabs and Footings under Concentrated Loads*; Portland Cement Association, Research and Development Laboratories: Skokie, IL, USA, 1961.

14. Adetifa, B.; Polak, M.A. Retrofit of slab column interior connections using shear bolts. *ACI Struct. J.* **2005**, *102*, 268.
15. Polak, M. Increasing Punching Strength and Ductility of Existing Reinforced Concrete Slab-Column Connections Against Abnormal Loading. In Proceedings of the Structures Congress 2005: Metropolis and Beyond, New York, NY, USA, 20–24 April 2005; pp. 1–6.
16. Saleh, H.; Kalfat, R.; Abdouka, K.; Al-Mahaidi, R. Experimental and numerical study into the punching shear strengthening of RC flat slabs using post-installed steel bolts. *Constr. Build. Mater.* **2018**, *188*, 28–39. [CrossRef]
17. Binici, B.; Bayrak, O. Punching shear strengthening of reinforced concrete flat plates using carbon fiber reinforced polymers. *J. Struct. Eng.* **2003**, *129*, 1173–1182. [CrossRef]
18. Sissakis, K.; Sheikh, S.A. Strengthening concrete slabs for punching shear with carbon fiber-reinforced polymer laminates. *ACI Struct. J.* **2007**, *104*, 49.
19. Erdogan, H.; Binici, B.; Ozcebe, G. Punching shear strengthening of flat-slabs with CFRP dowels. *Mag. Concr. Res.* **2010**, *62*, 465–478. [CrossRef]
20. Meisami, M.H.; Mostofinejad, D.; Nakamura, H. Punching shear strengthening of two-way flat slabs using CFRP rods. *Compos. Struct.* **2013**, *99*, 112–122. [CrossRef]
21. Meisami, M.H.; Mostofinejad, D.; Nakamura, H. Strengthening of flat slabs with FRP fan for punching shear. *Compos. Struct.* **2015**, *119*, 305–314. [CrossRef]
22. El-Salakawy, E.; Soudki, K.; Polak, M.A. Punching shear behavior of flat slabs strengthened with fiber reinforced polymer laminates. *J. Compos. Constr.* **2004**, *8*, 384–392. [CrossRef]
23. Polies, W.; Ghrib, F.; Sennah, K. Rehabilitation of interior reinforced concrete slab–column connections using CFRP sheets. *Constr. Build. Mater.* **2010**, *24*, 1272–1285. [CrossRef]
24. Sharaf, M.H.; Soudki, K.A.; Van Dusen, M. CFRP strengthening for punching shear of interior slab–column connections. *J. Compos. Constr.* **2006**, *10*, 410–418. [CrossRef]
25. Soudki, K.; El-Sayed, A.K.; Vanzwol, T. Strengthening of concrete slab-column connections using CFRP strips. *J. King Saud Univ.-Eng. Sci.* **2012**, *24*, 25–33. [CrossRef]
26. Aghayari, R.; Moradi, M. Improving the punching shear strength of RC slabs by FRP and steel sheets. *J. Rehabil. Civ. Eng.* **2016**, *4*, 1–17.
27. Ricker, M.; Häusler, F.; Hegger, J. Punching of edge column–slab connections–comparison of tests and codes. *Proc. Inst. Civ. Eng.-Struct. Build.* **2022**, *175*, 202–214. [CrossRef]
28. Robertson, I.N.; Durrani, A.J. Gravity load effect on seismic behavior of exterior slab-column connections. *Struct. J.* **1991**, *88*, 255–267.
29. Moehle, J.P.; Kreger, M.E.; Leon, R. Background to recommendations for design of reinforced concrete slab-column connections. *Struct. J.* **1988**, *85*, 636–644.
30. Moehle, J.P. Strength of slab-column edge connections. *Struct. J.* **1988**, *85*, 89–98.
31. Luo, Y.; Durrani, A. Equivalent Beam Model for Flat-Slab Buildings–Part II: Exterior Connections. *Struct. J.* **1995**, *92*, 250–257.
32. Moradi, M.; Daneshvar, K.; Ghazi-Nader, D.; Hajiloo, H. The prediction of fire performance of concrete-filled steel tubes (CFST) using artificial neural network. *Thin-Walled Struct.* **2021**, *161*, 107499. [CrossRef]
33. Park, H.G.; Choi, K.K. Strength of exterior slab–column connections subjected to unbalanced moments. *Eng. Struct.* **2007**, *29*, 1096–1114. [CrossRef]
34. Bu, W. Punching Shear Retrofit Method Using Shear Bolts for Reinforced Concrete Slabs under Seismic Loading. Ph.D. Thesis, University of Waterloo, Waterloo, ON, Canada, 2008.
35. Wang, W.; Zhang, D.; Lu, F.; Wang, S.C.; Tang, F. Experimental study on scaling the explosion resistance of a one-way square reinforced concrete slab under a close-in blast loading. *Int. J. Impact Eng.* **2012**, *49*, 158–164. [CrossRef]
36. Sadraie, H.; Khaloo, A.; Soltani, H. Dynamic performance of concrete slabs reinforced with steel and GFRP bars under impact loading. *Eng. Struct.* **2019**, *191*, 62–81. [CrossRef]
37. Kumar, V.; Kartik, K.; Iqbal, M.A. Experimental and numerical investigation of reinforced concrete slabs under blast loading. *Eng. Struct.* **2020**, *206*, 110125. [CrossRef]
38. Concrete Society Technical Report 55. *Design Guidance for Strengthening Concrete Structures Using Fibre Composite Materials*; The Concrete Society: Crowthorne, UK, 2000.
39. Daneshvar, K.; Moradi, M.J.; Ahmadi, K.; Mahdavi, G.; Hariri-Ardebili, M.A. Dynamic behavior of corroded RC slabs with macro-level stochastic finite element simulations. *Eng. Struct.* **2021**, *239*, 112056. [CrossRef]
40. Moradi, M.J.; Aghayari, R. Assessment the Effective Parameters on Punching Shear in Slab-Column Connections and Strengthed with FRP. *Modares Civ. Eng. J.* **2015**, *15*, 93–104.
41. Daneshvar, K.; Moradi, M.J.; Amooie, M.; Chen, S.; Mahdavi, G.; Hariri-Ardebili, M.A. Response of low-percentage FRC slabs under impact loading: Experimental, numerical, and soft computing methods. In *Proceedings of the Structures*; Elsevier: Amsterdam, The Netherlands, 2020; Volume 27, pp. 975–988.
42. Akhaveissy, A.; Daneshvar, K.; Ghazi-Nader, D.; Amooie, M.; Moradi, M.J. Numerical study on seismic behavior of composite shear walls with steel-encased profiles subjected to different axial load. *Pract. Period. Struct. Des. Constr.* **2021**, *26*, 04021034. [CrossRef]

43. Zhang, W.; Liu, X.; Huang, Y.; Tong, M.N. Reliability-based analysis of the flexural strength of concrete beams reinforced with hybrid BFRP and steel rebars. *Arch. Civ. Mech. Eng.* **2022**, *22*, 171. [CrossRef]
44. Huang, H.; Huang, M.; Zhang, W.; Guo, M.; Chen, Z.; Li, M. Progressive collapse resistance of multistory RC frame strengthened with HPFL-BSP. *J. Build. Eng.* **2021**, *43*, 103123. [CrossRef]
45. Hao, R.B.; Lu, Z.Q.; Ding, H.; Chen, L.Q. A nonlinear vibration isolator supported on a flexible plate: analysis and experiment. *Nonlinear Dyn.* **2022**, *108*, 941–958. [CrossRef]
46. Huang, H.; Guo, M.; Zhang, W.; Zeng, J.; Yang, K.; Bai, H. Numerical investigation on the bearing capacity of RC columns strengthened by HPFL-BSP under combined loadings. *J. Build. Eng.* **2021**, *39*, 102266. [CrossRef]
47. ABAQUS Documentation and User Manual, Version 6.10. *Dassault Syst.* **2010**.
48. Zhang, H.; Xiang, X.; Huang, B.; Wu, Z.; Chen, H. Static homotopy response analysis of structure with random variables of arbitrary distributions by minimizing stochastic residual error. *Comput. Struct.* **2023**, *288*, 107153. [CrossRef]
49. Li, J.; Wang, Z.; Zhang, S.; Lin, Y.; Wang, L.; Sun, C.; Tan, J. A novelty mandrel supported thin-wall tube bending cross-section quality analysis: A diameter-adjustable multi-point contact mandrel. *Int. J. Adv. Manuf. Technol.* **2023**, *124*, 4615–4637. [CrossRef]
50. Wang, Z.; Zhou, T.; Zhang, S.; Sun, C.; Li, J.; Tan, J. Bo-LSTM based cross-sectional profile sequence progressive prediction method for metal tube rotate draw bending. *Adv. Eng. Inform.* **2023**, *58*, 102152. [CrossRef]
51. Daneshvar, K.; Moradi, M.; Khaleghi, M.; Rezaei, M.; Farhangi, V.; Hajiloo, H. Effects of impact loads on heated-and-cooled reinforced concrete slabs. *J. Build. Eng.* **2022**, *61*, 105328. [CrossRef]
52. Wu, Z.; Huang, B.; Fan, J.; Chen, H. Homotopy based stochastic finite element model updating with correlated static measurement data. *Measurement* **2023**, *210*, 112512. [CrossRef]
53. Daneshvar, K.; Moradi, M.; Ahmadi, K.; Hajiloo, H. Strengthening of corroded reinforced concrete slabs under multi-impact loading: Experimental results and numerical analysis. *Constr. Build. Mater.* **2021**, *284*, 122650. [CrossRef]
54. Labibzadeh, M. The numerical simulations of the strengthened RC slabs with CFRPs using standard CDP material model of Abaqus code. *Eur. J. Environ. Civ. Eng.* **2015**, *19*, 1268–1287. [CrossRef]
55. Cui, W.; Zhao, L.; Ge, Y.; Xu, K. A generalized van der Pol nonlinear model of vortex-induced vibrations of bridge decks with multistability. *Nonlinear Dyn.* **2023**, *112*, 259–272. [CrossRef]
56. Ding, H.; Chen, L.Q. Shock isolation of an orthogonal six-DOFs platform with high-static-low-dynamic stiffness. *J. Appl. Mech.* **2023**, *90*, 111004.
57. Halabi, Z.; Ghrib, F.; El-Ragaby, A.; Sennah, K. Behavior of RC slab-column connections strengthened with external CFRP sheets and subjected to eccentric loading. *J. Compos. Constr.* **2013**, *17*, 488–496. [CrossRef]
58. El-Enein, H.A.; Azimi, H.; Sennah, K.; Ghrib, F. Flexural strengthening of reinforced concrete slab–column connection using CFRP sheets. *Constr. Build. Mater.* **2014**, *57*, 126–137. [CrossRef]
59. Zhou, C.; Wang, J.; Shao, X.; Li, L.; Sun, J.; Wang, X. The feasibility of using ultra-high performance concrete (UHPC) to strengthen RC beams in torsion. *J. Mater. Res. Technol.* **2023**, *24*, 9961–9983. [CrossRef]
60. Marcinczak, D.; Trapko, T.; Musiał, M. Shear strengthening of reinforced concrete beams with PBO-FRCM composites with anchorage. *Compos. Part B Eng.* **2019**, *158*, 149–161. [CrossRef]
61. Khaleghi, M.; Salimi, J.; Farhangi, V.; Moradi, M.J.; Karakouzian, M. Evaluating the behaviour of centrally perforated unreinforced masonry walls: Applications of numerical analysis, machine learning, and stochastic methods. *Ain Shams Eng. J.* **2022**, *13*, 101631. [CrossRef]
62. Lu, Z.; Brennan, M.; Ding, H.; Chen, L. High-static-low-dynamic-stiffness vibration isolation enhanced by damping nonlinearity. *Sci. China Technol. Sci.* **2019**, *62*, 1103–1110. [CrossRef]
63. Shu, Z.; Ning, B.; Chen, J.; Li, Z.; He, M.; Luo, J.; Dong, H. Reinforced moment-resisting glulam bolted connection with coupled long steel rod with screwheads for modern timber frame structures. *Earthq. Eng. Struct. Dyn.* **2023**, *52*, 845–864. [CrossRef]
64. ACI Committee 318. *Building Code Requirements for Structural Concrete (ACI 318-08) and Commentary*; American Concrete Institute: Farmington Hills, MI, USA, 2008.